American Society of Mechanical Engineers

ASME Pre-Print (Before Review) Repository

Institutional Repository Cover Sheet

Ecole Polytechnique Fédérale de Lausanne, Switzerland
Infoscience (https://infoscience.epfl.ch/)
https://infoscience.epfl.ch/record/282782

Patrick Hubert	Wagner	mail@patrick-wagner.net
First	*Last*	*E-mail*

ASME Paper Title: Influence of Large Relative Tip Clearances for a Micro Radial Fan and Design Guidelines for Increased Efficiency

Authors: Patrick Hubert Wagner, Jan Van herle, Lili Gu, Jürg Schiffmann

ASME Journal Title: ASME Turbo Expo 2020: Turbomachinery Technical Conference and Exposition
September 21–25, 2020
Virtual, Online

Paper No°: GT2020-15994, V008T20A025; 16 pages **Date of Publication (VOR* Online):** January 11, 2021

ASME Digital Collection URL:
https://asmedigitalcollection.asme.org/GT/proceedings-abstract/GT2020/84195/V008T20A025/1095155

DOI: https://doi.org/10.1115/GT2020-15994

*VOR (version of record)

ASME ©; CC-BY distribution license

Proceedings of the ASME 2020 Turbomachinery Technical Conference & Exposition
Turbomachines for Clean Power and Propulsion Systems
Turbo Expo 2020
June 22 - 26, 2020, London, England

GT2020-3836

DRAFT: INFLUENCE OF LARGE RELATIVE TIP CLEARANCES FOR A MICRO RADIAL FAN AND DESIGN GUIDELINES FOR INCREASED EFFICIENCY

Patrick H. Wagner

Laboratory for Applied Mechanical Design
Institute of Mechanical Engineering
École Polytechnique Fédérale de Lausanne
Neuchâtel, Neuchâtel, 2000
Switzerland
Email: patrick.wagner@epfl.ch

Jan Van herle

Group of Energy Materials
IGM
EPFL
Sion, Valais, 1951
Switzerland
Email: jan.vanherle@epfl.ch

Lili Gu, Jürg Schiffmann*

LAMD
IGM
EPFL
Neuchâtel, Neuchâtel, 2000
Switzerland
Email: lili.gu@epfl.ch
Email: jurg.schiffmann@epfl.ch

ABSTRACT

A radial fan with a tip diameter of 19.2 mm *and a constant blade height of* 1.82 mm *was tested with a running tip clearance of* 0.14 mm *and* 0.04 mm*. This corresponds to a relative clearance (blade tip clearance divided by blade height) of 0.077 and 0.022, respectively. With respect to the baseline operating conditions (rotational speed of* 168 krpm*, air mass flow rate of* 5.3 kg h^{-1}*, and total inlet temperature of* 200 °C*) the fan total-to-total pressure rise could be increased by* 20 mbar *to* 68 mbar*, by reducing the tip clearance. The isentropic total-to-total efficiency increased thus from* 53 % *to* 64 %*, suggesting a significant impact of the blade tip clearance for such a micro radial fan. A single passage CFD simulation correlates well to these observations. The widely-used Pfleiderer correlation with an empirical coefficient of 2.8 fits the simulation and experiments within* ± 2 *efficiency points. The authors suggest three measures to mitigate the blade tip clearance losses for small-scale fans: (1) gas-bearing supported rotors (here: herringbone-grooved journal bearings and a single-sided spiral-grooved thrust bearing) to realize low blade tip clearances of down to* 0.040 mm*, due to the tight bearing tolerances, (2) a mid-loaded blade design, and (3) unloading the fan leading edge, and thus reducing the blade tip clearance vortex in the fan passage.*

NOMENCLATURE

a	Speed of sound in m s^{-1}
b	(Channel) width in m
c	Absolute velocity in m s^{-1}
d	Diameter in m
d_s	Specific diameter
h	Specific enthalpy in J kg^{-1} K^{-1}
H	Blade height in m
Ma	(Blade tip) Mach number
$\dot{m}$	Mass flow rate in kg s^{-1}
n_s	Specific speed
P	Power in W
p	Pressure in Pa
r	Radius in m
Re_d	Reynolds number based on the tip diameter
Re_b	Reynolds number based on the TE channel width
s	Specific entropy in J kg^{-1} K
S	Blade tip clearance in m
T	Temperature in K
$\dot{V}$	Volume flow rate in m^3 s^{-1}
u	Circumferential velocity in m s^{-1}
α	Absolute blade angle based on the circumference in rad
β	Relative blade angle based on the circumference in rad
ζ	Experience coefficient

*Address all correspondence to this author.

Copyright © 2020 by ASME

η Efficiency
θ Blade wrap angle in rad
ρ Density in $\mathrm{kg\,m^{-3}}$
κ heat capacity ratio
ϕ Flow coefficient
ψ Work coefficient
ω Angular speed in $\mathrm{rad\,s^{-1}}$

Subscript

1 machine inlet / inlet side test section
3 fan blade leading edge
4 fan blade trailing edge
6 volute outlet
8 machine outlet / outlet side test section
is isentropic
nom nominal condition
m meridional
pol polytropic
st static
t total
u circumferential

Abbreviation

CFD computational fluid dynamics
FP full passage
LE leading edge
SP single passage
TE trailing edge

INTRODUCTION

Due to constraints in manufacturing and assembling, the minimum-achievable absolute blade tip clearance in turbomachines is limited. Furthermore, the blade tip clearance changes during operation, due to: (1) axial and radial shaft motion, (2) thermal expansion, and (3) mechanical blade deformation. The cold blade tip clearance at zero rotational speed, therefore, is not equal to the hot tip clearance at the nominal operation. Commercial turbochargers with floating ring hydrostatic oil bearings achieve an absolute tip clearance of down to 0.1 mm. Schiffmann and Favrat [1] tested a radial compressor with a tip clearance of 0.04 mm, using dynamic gas bearings, i.e., herringbone-grooved and spiral-grooved thrust bearings. Sato et al. [2] tested a micro-sized radial-inflow turbine and adjusted the tip clearance with an "trial-and-error" method, using different shim sizes, which were incremented by 0.025 mm. The shim was chosen in such way, that no contact between the blades and the shroud occurred at the nominal point; hence, the maximum blade tip clearance was lower than 0.025 mm. The turbine shaft was supported on ball bearings.

Due to these limitations, the relative blade tip clearance, i.e., the ratio of the absolute tip clearance divided by the blade height (S/H), is limited for small-scale turbomachines. The blade tip clearance secondary loss is suggested to be the most dominant one for small-scale turbomachines. An exact determination of this loss is thus essential for a small-scale turbomachine pre-design. [3]

Analytical correlations: The centrifugal compressor and pump literature, provides several empirical blade tip clearance loss models. These correlations are commonly expressed with the relative blade tip clearance (S/H). In 1953, Eckert and Schnell [4] suggested a linear model. The decrease of the total-to-total isentropic efficiency

$$\Delta\eta_{is,tt} = -\zeta\,\eta_{is,tt,nom}\frac{2S}{H_3+H_4} \tag{1}$$

is suggested to be a function of the nominal efficiency ($\eta_{is,tt,nom}$), the relative blade tip clearance ($2S/(H_3+H_4)$), and an empirical factor (ζ), which was determined to 0.9. In 1955, Pfleiderer [5] introduced a similar correlation for the efficiency correction with an empirical factor ranging from 1.5 to 3, valid for radial pumps. In 1968, Schmidt-Theuner and Mattern [6] investigated a radial compressor with a vaned diffuser and presented a non-linear correlation

$$\Delta\eta_{pol} = -0.23\frac{S_4}{H_4} + 0.46\left(\frac{S_4}{H_4}\right)^2 \quad 0.035 < \frac{S}{H_4} < 0.14 \tag{2}$$

valid for relative blade tip clearance ratios between 3.5 % and 14 %. The Reynolds numbers (based on the tip diameter of 355 mm) ranged from 2.2×10^6 to 12.1×10^6. In 1980, Musgrave [7] published another linear correlation, based on the experimental data from Pampreen. [8]

$$\Delta\eta_{is} = 0 \qquad \frac{S_4}{H_4} \le 0.03 \tag{3}$$

$$\Delta\eta_{is} = -0.35\frac{S_4}{H_4} + 0.01 \qquad \frac{S}{H_4} > 0.03 \tag{4}$$

In 1985, Ganter [9] further refined the empirical factor (ζ) in eq. (1) for radial pumps and suggested a coefficient of 1 to 3.5, depending on the specific speed and the clearance ratio. Thus, this correlation is also non-linear. In 2019, Diehl and Schiffmann [10] suggested that the tip clearance effect further depends on the compressor operating point, i.e. the tip clearance effect is less pronounced towards surge and vice versa for an operation close to choking conditions.

Shimming and trimming: Generally, there are two different methodologies for investigating the blade tip clearance effect: the shimming and the trimming approach. The shimming approach is easy-to-implement and cost-efficient. The trimming

Copyright © 2020 by ASME

approach is certainly the more accurate one, since the channel width is kept constant, and thus the flow diffusion and the outlet meridional velocity is constant. However, this approach is also more expensive to implement experimentally, since for each new test case, a fan impeller with a different blade height is necessary. Another disadvantage of this approach is, that the fan impeller manufacturing and assembling tolerances can lead to a perturbation of the investigated tip clearance effect. This is significant, especially for small-scale turbomachines, where an exact axial alignment of the fan impeller hub is challenging.
Diehl [11] implemented the trimming approach for a 4.6-times up-scaled radial compressor with a diameter of 15 mm, designed by Javed et al. [12]. This allowed for an investigation of the small-scale compressor, since, according to Diehl, the blade tip clearance is Reynolds-independent. In this work, the shimming approach is implemented.

The scope of this paper is the experimental and numerical investigation of the blade tip clearance effect of a small-scale fan with a tip diameter of 19.2 mm, operating at a Reynolds number based on its tip diameter of 0.9×10^5. The results are compared to empirical loss correlations found in the literature. Furthermore, the authors compare the experimental result to pre-design concepts based on similarity concepts and provide design guidelines to minimize the tip clearance effects for small-scale fans.

FAN DESIGN SUMMARY

Wagner et al. [13] presented the characterization of a recirculation fan with a tip diameter of 19.2 mm, lubricated on dynamic gas bearings, i.e., herringbone-grooved journal and spiral-grooved thrust bearings. The fan features four prismatic main and splitter blades, which are highly backward-curved ($\beta_{4,blade} = 17°$) and have a constant height of 1.82 mm. The initial characterization featured a 0.1 mm shim, that increased the nominal blade tip clearance from 0.05 mm to 0.15 mm. Due to the axial motion of the shaft during operation, the tip clearance is reduced by 0.01 mm to 0.14 mm at the nominal speed of 168 krpm. This corresponds to a running relative blade tip clearance ($\frac{S_4}{H_4} = \frac{0.14}{1.82}$) of 0.077. Mitigating tip leakage and the associated secondary flow losses is beneficial for the fan efficiency. Generally, a tip leakage vortex forms at the blade leding egde (LE) and then stretches through the entire impeller domain. This vortex forms due to the pressure difference between the blade suction and pressure side. A reduction of this pressure difference at the blade LE, where the most dominant vortex starts, reduces therefore the intensity of the tip leakage vortex. The fan total-to-total pressure rise over a certain blade length at the point (P) is zero, if the Euler work,

$$\Delta h_{tt,3,P} = c_{u,P} u_P - c_{u,3} u_3 \stackrel{!}{=} 0 \tag{5}$$

is also zero. A blade designed with eq. (5) has, therefore, no total pressure rise. Assuming conservation of momentum ($c_u r =$ const.) and conservation of mass ($2\pi r b c_m =$ const.), the blade wrap angle (θ) for a zero-Euler-work blade [14],

$$\theta(r) = \frac{1}{2} \frac{u_3}{c_{m,1}} \left[\left(\frac{r}{r_3} \right)^2 - 1 \right] - \frac{c_{u,3}}{c_{m,3}} \ln \frac{r}{r_3} \tag{6}$$

is a function of the inlet conditions at the blade LE ($c_{m,3}$, $c_{u,3}$, r_3, and u_3) and the fan radius (r). In the case of no inlet swirl ($c_{u,3} = 0$) and close-to-radial blades ($dm \approx dr \longrightarrow \beta_{blade}(r) \approx \arctan \frac{dr}{r d\theta}$), the relation for the blade angle

$$\beta_{blade}(r) \approx \arctan \left[\frac{r_3 c_{m,3}}{u_3 r} \left(\frac{2\theta c_{m,3}}{u_3} + 1 \right)^{-0.5} \right] \tag{7}$$

is a function of the radius (r) and the following LE values (fan section 3): radius (r_3), the meridional velocity ($c_{m,3}$), and the circumferential velocity (u_3).
The presented fan design is unloaded at the first 22 % of the meridional coordinate according to eq. (7). Within this region, the Euler work is zero, and as a result, the total pressure rise is approximately zero in the inducer region.

MEASUREMENT SETUP

The measurement setup and equipment is similar to the one described by Wagner et al. [13]. However a *Scanivalve* DSA 3217 (6.9 bar) with a verified measurement uncertainty of ± 0.02 % on the full scale (± 0.7 mbar) was used to measure the fan TE pressure at a diameter of 18.55 mm at three different positions (240°, 120°, and 0°, corresponding to the end of the fan volute). This allows for a more accurate fan TE static pressure measurement (previous measurement uncertainty of ± 3.1 mbar).

NUMERICAL SETUP

Both steady full passage (FP) and a single passage (SP) computational fluid dynamics (CFD) simulations are preformed. Wagner et al. [13] used a FP simulation model with an unstructured mesh, including the fan impeller and the volute, instead of a SP model without volute. This approach was necessary for obtaining good correlation with the experiments, due to the significant pressure loss in the volute. A total pressure measurement at the fan TE would allow to compare a simulation model without volute to the experiments. However, such a measurement is challenging for a small-scale fan and only the static pressure with three evenly-distributed pressure taps was measured. Additionally, at this point, transient effects due to the blade passing are

Copyright © 2020 by ASME

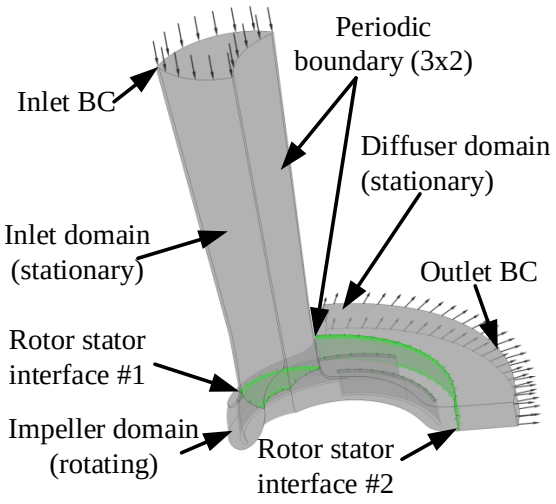

FIGURE 1: DOMAIN REGIONS OF THE SINGLE PASSAGE CFD SIMULATION: INLET, ROTATING FAN IMPELLER WITH MAIN AND SPLITTER BLADE, AND VIRTUAL DIFFUSER WITH ROTATING HUB (FROM LEFT TO RIGHT). THE FLUID-TO-FLUID INTERFACES BETWEEN THE STATIONARY AND ROTATING DOMAIN ARE MARKED GREEN.

much more dominant, what limits the accuracy of a steady simulation. Thus, the outlet static pressure was measured with four evenly-distributed pressure taps downstream of the volute and the diffusor in a pipe with a diameter of 12 mm. The FP CFD simulation suggests that the losses in the volute can be modeled by assuming that 60 % of the circumferential absolute velocity at the fan TE ($c_{u,4}$) and 100 % of the meridional velocity ($c_{m,4}$) is dissipated, due to the swirling motion of the fluid.

$$\Delta p_{loss,64} = \frac{1}{2}\rho_4 \left(c_{m,4}^2 + 0.6 c_{u,4}^2\right) \tag{8}$$

Thus, it is possible to estimate the total-to-total pressure rise and total-to-total isentropic efficiency with a SP model without volute, by taking into account the volute losses according to eq. (8).

Figure 1 shows the geometric fan model, consisting of an inlet duct, the transition region to the inducer inlet with a tangent Haack nose cone, the single passage impeller with the main and splitter blade (section 3 to 4), and an additional diffuser. The addition of the virtual diffuser helps the simulation to achieve a better convergence. The fan diffuser is therefore a numerical virtual domain that does not represent the real system. The diffuser walls are modeled as free-slip wall.

TABLE 1: RUNNING BLADE TIP CLEARANCE (S_4) IN mm, RELATIVE BLADE TIP CLEARANCE (S_4/H_4), NUMBER OF LAYERS IN TIP CLEARANCE, AND TOTAL NUMBER OF MESH ELEMENTS FOR THE FIVE DIFFERENT CASES. **BOLD** CLEARANCES WERE INVESTIGATED EXPERIMENTALLY.

S_4 in mm	S_4/H_4	Nr. of layers in tip clearance	Total nr. of mesh elements
0	0/1.82=0	0	0.79m
0.04	0.04/1.82=0.022	9	1.00m
0.09	0.09/1.82=0.049	19	1.24m
0.14	0.14/1.82=0.077	29	1.55m
0.24	0.24/1.82=0.132	50	2.05m

Grid generation: In total, two different fluids (hot air and anode off-gas at 200 °C) and five different blade tip clearances for the nominal blade height (H_4) of 1.82 mm were investigated: a zero tip clearance (ideal case), the nominal tip clearance of 0.04 mm (at the nominal speed), and three additional blade tip clearances (S_4) of 0.09 mm, 0.14 mm, and 0.24 mm, that are realized with a shim of 0.05 mm, 0.1 mm, and 0.2 mm thickness, respectively. This results in relative tip clearances (S_4/H_4) of 0, 0.022, 0.049, 0.077, and 0.132, respectively. The mesh is the same for the all ten cases, except that the number of cells within the tip clearance increases linearly from 0 to 50. Thus, the total mesh element number is not constant for all investigated cases. Table 1 lists the parameters of the five different tip clearance cases.
For the ten cases, the first element height was set 0.0005 mm, which corresponds to an average y^+ value well below 1.0. The maximum y^+ value of the first cell (1.54) occurs for the simulation with a blade tip clearance of zero and the anode off-gas, whereas it is 1.26 for hot air. For all other cases, the maximum y^+ value is below 1.2. However, the maximum y^+ value only occurs locally; for example, at the main and splitter blade LE.

Boundary conditions: Figure 1 shows the simulation boundary conditions. The inlet boundary conditions are the total temperature (200 °C), the total pressure (0.96 bar), and the gas composition. Two different gases are investigated corresponding to the experimental results and the actual application, respectively: hot air at 200 °C and the anode off-gas at 200 °C (molar ratios of water vapor, hydrogen, carbon monoxide, and carbon dioxide of 61.4 %, 7.4 %, 2.6 %, and 28.6 %, respectively). The numerical tip clearance study uses the conditions of the experi-

Copyright © 2020 by ASME

mental results with hot air by Wagner et al. [13]. The rotational speed is 168 krpm and the mass flow rate is 5.3 $\mathrm{kg\,h^{-1}}$ (outlet boundary condition). Based on a constant blade tip Mach number (calculated with the total inlet conditions) of 0.39

$$Ma_{t,4} = \frac{\omega d_4}{2a_{t,1}} \tag{9}$$

and a constant flow coefficient (calculated with the total inlet conditions) of 0.033

$$\Phi_{t,1} = \frac{2\dot{m}_1}{d_4^3 \omega \rho_{t,1}} \tag{10}$$

the boundary conditions for the anode off-gas case are determined to 175.5 krpm and 4.71 $\mathrm{kg\,h^{-1}}$.
Further boundary conditions are as follows:

- The rotor-stator interfaces #1 and #2 is a fluid-to-fluid frozen rotor interfaces.
- The impeller domain rotates at the rotational speed.
- The fan hub and the fan blades are rotating no-slip walls, whereas the fan shroud is a counter-rotating no-slip wall to account for the relative motion of fan blades and hub.
- All sides of the fluid domain are rotational periodicities (in total 3x2) to account for the interaction of the different single passages.
- The blade clearance interfaces are a fluid-to-fluid interfaces.

Solver setup: The CFD simulation uses compressible fluids with constant heat capacity and viscosity at 200 °C. The heat transfer model accounts for the fluid total energy. The advection scheme is high resolution for all differential equations. The shear stress transport model with a low turbulence intensity of 1 % at the inlet boundary accounts for the fluid turbulence.

BLADE LOADING

According to Diehl [11], the blade shape and the resulting blade loading have a more significant impact on the blade tip clearance secondary loss effect, as the relative clearance increases. While stating the blade tip clearance effect, it is thus important to specify the exact blade-loading (mid-loaded in this case).

Blade shape: Figure 2 shows the blade angle (β_{blade}) distribution at the fan hub that is equal to a span of 0 (blue line with squares), at a span of 0.5 (blue line with dots), and at the shroud that is equal to a blade span of 1 (blue line with circles). The blade angle distribution of the first 22 % with respect to the meridional coordinate follows eq. (7) (blue line with squares in the lower graph of Figure 2). Within this region, the Euler work is zero, and as a result, the total pressure rise is approximately zero. The blue line with the hexagrams shows the blade angle distribution at the main blade LE. The blade angle varies between 36° at the hub (radius of 3.7 mm) and 30° at the shroud (radius of 5 mm). The vertical black dashed lines mark the main blade LE at the hub and at the shroud, the splitter blade LE, as well as the main and splitter blade TE.

Blade loading: Figure 2 shows single passage CFD results of the fan impeller for the case with hot air at 200 °C and a running blade tip clearance of 0.14 mm. The static pressure at the main blade, as well as at the splitter blade suction and pressure side are represented by red dots. At the hub surface (0 span) and at a span of 0.5, the static pressure is near-constant until the splitter blade LE at a radius of 6.35 mm (due to the zero-Euler-work blade design). Between the splitter blade LE and the blade TE, the pressure rises linearly within the fan impeller, which leads to a pressure difference between the blade suction and pressure side, which is pronounced at a span of 0.5. The pressure difference at a span of 0.92 is within a few mbar at the radius of 5.5 mm.
Because of the blade LE thickness of 0.25 mm, the flow decelerates at the blade stagnation point, leading to a high static pressure. On the blade suction surface a local separation forms with a low static pressure, since the flow cannot follow the rapid geometrical change of the blade LE. On the blade pressure side, the pressure rises; hence, the pressure difference in this region is high (up to 15 mbar at a blade span of 0.92, as shown in the upper graph of Figure 2).

Blade tip leakage: Figure 3 shows the absolute velocity in the middle of the blade tip clearance (i.e., 0.5 blade tip clearance span) represented by green dots, as well as for different spans within the blade tip clearance (between 0 and 1). The absolute velocity (c) decreases from 44 $\mathrm{m\,s^{-1}}$ at the main blade LE to a minimal value of 30 $\mathrm{m\,s^{-1}}$ at a radius of 5.5 mm (minimum pressure difference between suction and pressure side). This decrease in absolute velocity at the blade LE is a result of the zero-Euler-work blade design, and limits the tip leakage mass flow rate, increasing the fan isentropic efficiency. For higher radii than 5.5 mm, the absolute velocity steadily increases towards a maximum value of 94 $\mathrm{m\,s^{-1}}$ at a radius of 8 mm. At this point, the highest pressure difference of 22 mbar between the blade suction and pressure side can be observed.

Blade incidence and deviation: Figure 2 also shows the mass-flow-averaged relative velocity angle (β) as a continuous green line. A comparison of β with the blade angle leads to the incidence at the blade LE and the deviation at the blade TE. At a span of 0.92 and 0.5, the incidence is thus positive and at +3°,

Copyright © 2020 by ASME

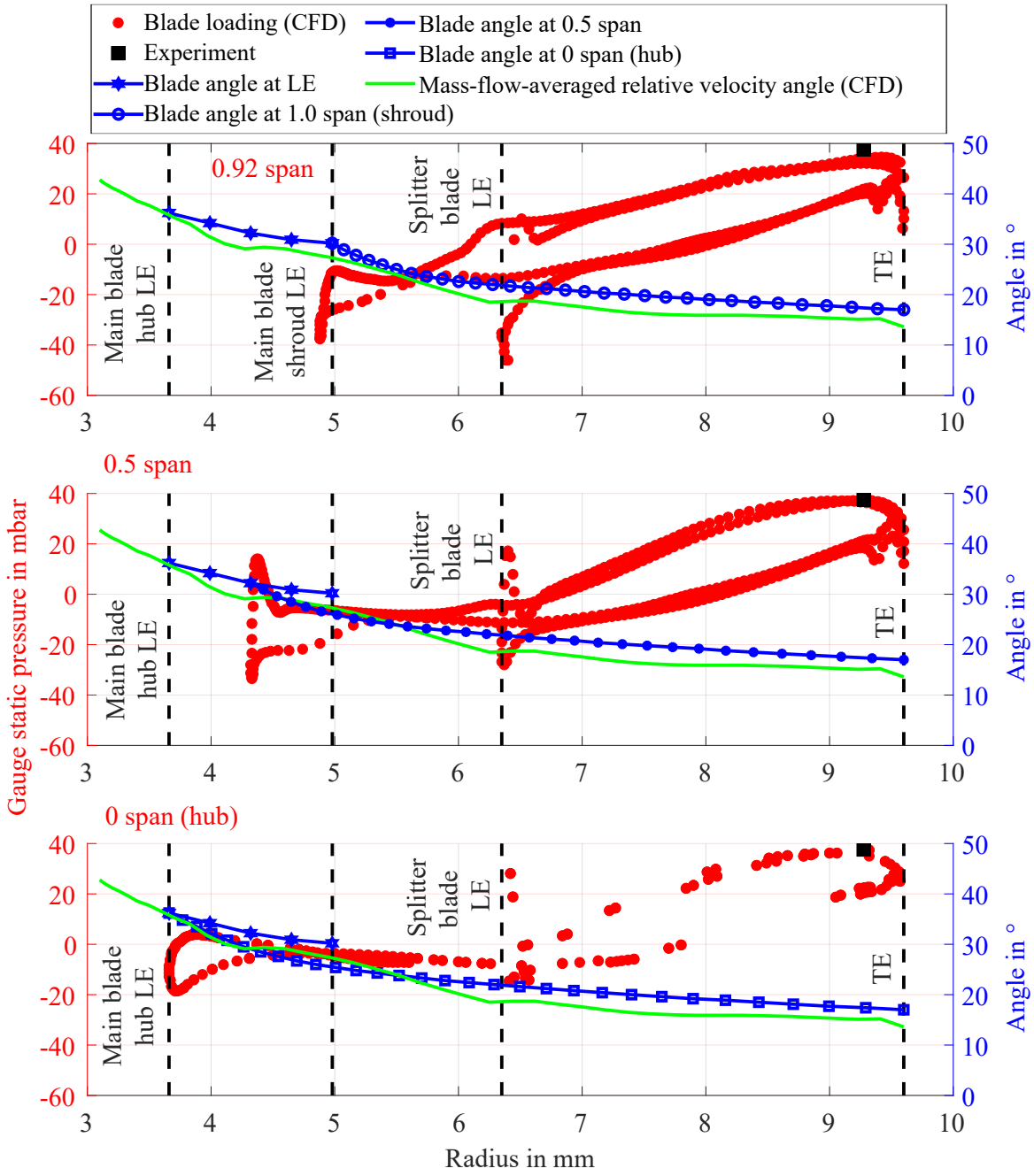

FIGURE 2: EXPERIMENTAL STATIC PRESSURE MEASUREMENT (BLACK SQUARE) AT THE SHROUD (RADIUS OF 9.28 mm) AND COMPUTATIONAL BLADE LOADING (RED POINTS) OF A FAN BLADE (THE RELATIVE TIP CLEARANCE IS 0.077 AND THE TIP IS LOCATED AT $1 - 0.071 = 0.929$ SPAN) AT DIFFERENT SPANS: 0.92 SPAN (UPPER GRAPH), 0.5 SPAN (MIDDLE GRAPH), AND ZERO SPAN (LOWER GRAPH). THE BLUE LINE CORRESPONDS TO THE BLADE ANGLE AT DIFFERENT SPANS: 1.0 SPAN (CIRCLES), 0.5 SPAN (DOTS), AND ZERO SPAN (SQUARES). THE LINE WITH HEXAGRAMS CORRESPONDS TO THE BLADE ANGLES AT THE FAN LEADING EDGE (LE). THE GREEN LINE SHOWS THE MASS-FLOW-AVERAGED RELATIVE VELOCITY ANGLE (β).

Copyright © 2020 by ASME

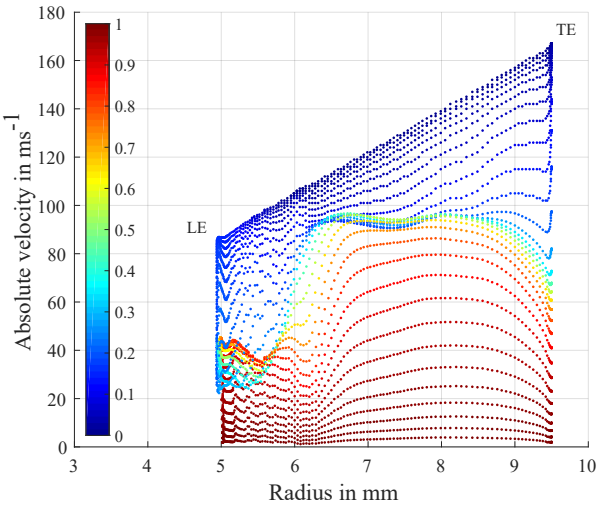

FIGURE 3: ABSOLUTE VELOCITY (c) OF HOT AIR AT 200 °C WITHIN THE BLADE TIP CLEARANCE AT DIFFERENT SPANS (ABSOLUTE BLADE TIP CLEARANCE IS 0.14 mm). AT 100 % BLADE TIP CLEARANCE SPAN, I.E., AT THE SHROUD SURFACE, THE VELOCITY IS ZERO BECAUSE OF THE COUNTER-ROTATING NO-SLIP WALL, WHEREAS THE VELOCITY IS EQUAL TO $u = \omega r$ AT THE BLADE TIP (I.E., AT ZERO BLADE TIP CLEARANCE SPAN), BECAUSE OF THE ROTATING NO-SLIP WALL.

whereas it is +0.5° at the hub. Upstream of the main blade LE at a span of 0.5 and in front of the splitter blade LE, β has an irregularity, since the flow conforms to the blades. Downstream of the splitter blade LE, the relative velocity angle is always smaller than the blade angle, which leads towards a deviation of 3° at the blade TE.

Comparison to the experiment: The graph also features a comparison with experimental results. The manufactured fan volute features three evenly-distributed pressure taps with a diameter of 0.4 mm. A low-frequency (3 Hz) pressure sensor measures the time-averaged static pressure at the fan shroud. The graph shows the average value of all three taps. This value (37.6 mbar) is 4.3 mbar higher than the line-averaged shroud static pressure at similar position (diameter of 18.55 mm), obtained from the single passage steady CFD simulation (33.3 mbar).

COMPARISON OF THE EXPERIMENTAL RESULTS TOWARDS THE NUMERICAL RESULTS AND THE EMPIRICAL CORRELATIONS

Table 2 lists the experimental and numerical results (both SP and FP CFD simulation). All listed values are evaluated using air with an inlet total temperature ($T_{t,1}$) of 200 °C, an inlet total pressure ($p_{t,1}$) of 0.96 bar, an impeller rotational speed of 168 krpm, and an inlet mass flow rate ($\dot{m}_1$) of 5.3 kg h^{-1}, corresponding to a volume flow rate of 125 l min^{-1}.

Evaluation of parameters: The fan inlet (1), TE (4), and outlet (8) pressures and temperatures are used to evaluate the total-to-total temperature difference (ΔT_{tt}), the power ($P = \dot{m}\Delta h_{tt}$), and the total-to-total isentropic efficiencies, assuming and adiabatic system ($T_{t,4} = T_{t,8}$).

$$\eta_{is,tt,81} = \frac{h_{is,t,8}\left[p_{t,8}, s\left(p_{t,1}, T_{t,1}\right)\right] - h_{t,1}\left(p_{t,1}, T_{t,1}\right)}{h_{t,8}\left(p_{t,8}, T_{t,8}\right) - h_{t,1}\left(p_{t,1}, T_{t,1}\right)} \tag{11}$$

$$\eta_{is,tt,41} = \frac{h_{is,t,4}\left[p_{t,4}, s\left(p_{t,1}, T_{t,1}\right)\right] - h_{t,1}\left(p_{t,1}, T_{t,1}\right)}{h_{t,4}\left(p_{t,4}, T_{t,4}\right) - h_{t,1}\left(p_{t,1}, T_{t,1}\right)} \tag{12}$$

Specific enthalpies and entropies are evaluated with a commercial fluid database. Table 2 includes the respective measurement uncertainties. The experiment evaluates the total-to-total pressure rise and efficiency between the machine inlet and the outlet ($\Delta p_{tt,81}$ and $\eta_{is,81}$, respectively), the SP simulation evaluates these values between the fan inlet and TE ($\Delta p_{tt,41}$ and $\eta_{is,41}$), and the FP simulation evaluates both cases. Equation (8) is used to evaluate the pressure loss between the fan TE and the volute outlet, what allows to estimate the pressure rise and isentropic efficiency over the entire machine ($\Delta p_{tt,81}$ and $\eta_{is,81}$, respectively) for the SP simulation. Additionally, the total-to-static pressure rise ($\Delta p_{tst,41}$) and efficiency

$$\eta_{is,tst,41} = \frac{h_{is,st,4}\left[p_{st,4}, s\left(p_{t,1}, T_{t,1}\right)\right] - h_{t,1}\left(p_{t,1}, T_{t,1}\right)}{h_{t,4}\left(p_{t,4}, T_{t,4}\right) - h_{t,1}\left(p_{t,1}, T_{t,1}\right)} \tag{13}$$

between the machine inlet (1) and fan blade TE (4) is evaluated for the experiments, SP and FP CFD simulation.

Hot air case: Table 2 lists the measurement results for the running blade tip clearance of both 0.14 mm (published in [13]) and 0.04 mm. Considering the 0.14 mm case, the SP and FP CFD simulation correlate well to the experiments in terms of the total-to-total temperature rise (12.5 °C ± 0.5 °C), and thus the fan power (18.8 ± 0.8). The total-to-total pressure rise between the machine inlet (1) and outlet (8) $\Delta p_{tt,8,1}$ is 48.7 mbar for the experiment, whereas it is 46.9 mbar and 46.6 mbar for the FP and SP simulation, respectively. This corresponds to a correlation within 5 %.
Considering the 0.04 mm case, the simulated temperature difference and power correlate to the measurements (14.4 °C and 21.7 W, respectively). The experimental pressure rise (68.3 mbar) correlates within 1 % to the estimated one (68.8 mbar) by the SP CFD simulation.
The experimentally-determined total-to-total pressure rise and

Copyright © 2020 by ASME

TABLE 2: COMPARISON OF EXPERIMENT (TOP), FULL PASSAGE (MIDDLE) WITH VOLUTE, AND SINGLE PASSAGE (BOTTOM) WITH VIRTUAL DIFFUSER CFD SIMULATIONS FOR HOT AIR AT A TOTAL INLET TEMPERATURE OF 200 °C, A TOTAL INLET PRESSURE OF 0.96 bar, A ROTATIONAL SPEED OF 168 krpm, AND A MASS FLOW RATE OF 5.3 kg h^{-1} WITH A TE DIAMETER OF 19.2 mm (CONSTANT H_4 OF 1.82 mm AND $\beta_{4,blade} = 17°$).

	S_4 in mm	b_4 in mm	$\Delta p_{tt,81}$ [a] in mbar	$\Delta p_{tt,41}$ [b] in mbar	$\Delta p_{tst,41}$ [b] in mbar	$\eta_{is,tt,81}$ [a] in %	$\eta_{is,tt,41}$ [b] in %	$\eta_{is,tst,41}$ [b] in %	P in W	ΔT_{tt} in K	Δs_{41} [b] in J kg^{-1} K^{-1}
SP	0.24	2.06	**33.3**[c]	44.0	20.6	**42.3**[c]	55.8	26.3	18.2	10.7	10.1
Exp. [13]	0.14	1.96	48.7 ± 0.15	-	37.6 ± 3.1	52.9 ± 2.1	-	41.0 ± 1.7	18.8 ± 0.8	12.5 ± 0.5	-
FP [13]	0.14	1.96	46.9	59.9	31.1	52.0	65.9	34.6	18.5	12.3	8.9
SP	0.14	1.96	**46.6**[c]	59.4	33.3	**51.5**[c]	65.3	37.0	18.5	12.3	9.0
SP	0.09	1.91	**56.3**[c]	70.2	43.8	**58.7**[c]	72.8	45.9	19.5	13.0	7.4
Exp.	0.04	1.86	68.3 ± 0.2	-	54.6 ± 0.7	64.0 ± 2.2	-	51.4 ± 1.8	21.7 ± 0.8	14.4 ± 0.5	-
SP	0.04	1.86	**68.8**[c]	85.6	55.2	**64.2**[c]	79.4	51.8	21.7	14.4	6.3
SP	0	1.82	**74.0**[c]	91.5	61.2	**66.2**[c]	81.4	55.1	22.6	15.0	5.9

[a] Evaluated between the machine inlet (1) and machine outlet (8) [b] Evaluated between the machine inlet (1) and fan blade TE (4)
[c] Estimated with the volute pressure loss (4-8) according to eq. (8)

power increased by 40 % and 15 %, respectively, resulting in an increase of the total-to-total isentropic efficiency by 21 % by reducing the tip clearance from 0.14 mm to 0.04 mm. Power and efficiency were measured as 21.7 W and 64 %, resulting in a pressure rise of 68.3 mbar for the 0.04 mm tip clearance case. With respect to the measured case with a blade tip clearance of 0.14 mm, the SP simulation suggest an increase by 10 mbar, 22 mbar, and 27 mbar for the 0.09 mm, 0.04 mm, and the (theoretical) 0 mm case.

Pressure rise for hot air and anode off-gas: Although the Mach number of both cases (hot air and anode off-gas) are the same, the pressure rise is lower for the anode off-gas case due to the lower heat capacity ratio (κ). For hot air it is 1.4, whereas it is 1.3 for the anode off-gas. With the definition of the work coefficient (ψ) and the total-to-total fan specific enthalpy rise ($\Delta h_{tt,fan} = \psi u_4^2 = \psi Ma_{t,4}^2 \kappa R T_{t,1}$), the total pressure at the fan outlet (section 8) can be calculated.

$$p_{t,8} = p_{t,1} \left[1 + (\kappa - 1)\, \psi Ma_{t,4}^2\right]^{\eta_{is,81} \frac{\kappa}{\kappa - 1}} \tag{14}$$

With respect to this equation, a fan with a constant work coefficient (ψ), a constant isentropic total-to-total efficiency ($\eta_{is,81}$), and a constant Mach number ($Ma_{t,4}$) achieves a higher pressure rise with a higher heat capacity ratio (κ), and vice versa.

Anode off-gas case: Wagner et al. [15] coupled the recirculation fan to a 6 kW_e solid oxide fuel cell system and operated it in the relevant environment. At the nominal blade tip clearance (0.4 mm), the fan was designed for a 10 kW_e fuel cell system for the following inlet conditions: a total pressure ($p_{t,1}$) of 1.05 bar, a total temperature ($T_{t,1}$) of 200 °C, a mass flow rate ($\dot{m}_1$) of 4.78 kg h^{-1}, and molar ratios of H_2O, H_2, CO, and CO_2 of 61.4 %, 7.4 %, 2.6 %, and 28.6 %, respectively. The design total-to-total pressure rise is 70 mbar at a rotational speed of 175.2 krpm. However, the test conditions were different: a 0.1 mm shim was inserted for risk mitigation and the fuel cell system power output was 6 kW_e, operated at a lower fuel utilization (0.85 instead of 0.925). The tested fan conditions, therefore, are different ($p_{t,1} = 0.99$ bar, $T_{t,1} = 192$ °C, $\dot{m}_1 = 2.8$ kg h^{-1}, and molar mass ratios of H_2O, H_2, CO, and CO_2 of 52.1 %, 14.6 %, 5.4 %, and 27.9 %, respectively). Thus, the fan was operated off-design at a lower mass flow rate, and a lower rotational speed. The experimental measurements and the CFD simulations of SP and FP are listed in Table 3 at the top. Pressure rise and power are underestimated by the CFD simulation. However, the total-to-total isentropic efficiency ($\eta_{is,tt,81}$) is comparable for the experiment (48 % ± 2 %), the FP simulation (51 %), and the SP simulation (55 %).
Table 3 at the bottom provides data for the tip clearance analysis with the anode off-gas. The mesh and simulation setup are identical to the hot air case analysis. As suggested, the blade TE Mach number and flow coefficient are constant with respect

Copyright © 2020 by ASME

TABLE 3: TOP: COMPARISON OF EXPERIMENT (EXP.), FULL PASSAGE (FP), AND SINGLE PASSAGE (SP) WITH VIRTUAL DIFFUSER CFD SIMULATIONS FOR ANODE OFF-GAS AT A TOTAL INLET TEMPERATURE OF 192 °C, A TOTAL INLET PRESSURE OF 0.99 bar, A ROTATIONAL SPEED OF 165.5 krpm, AND A MASS FLOW RATE OF 2.75 kg h^{-1}. BOTTOM: COMPARISON OF THE SP CFD SIMULATION FOR THE ANODE OFF-GAS WITH A TOTAL INLET TEMPERATURE OF 200 °C, A TOTAL INLET PRESSURE OF 0.96 bar, A ROTATIONAL SPEED OF 175.5 krpm, AND A MASS FLOW RATE OF 4.71 kg h^{-1}. THE TOP AND BOTTOM PART REFER TO A FAN WITH A TE DIAMETER OF 19.2 mm (CONSTANT H_4 OF 1.82 mm AND $\beta_{4,blade} = 17°$).

	S_4 in mm	b_4 in mm	$\Delta p_{tt,81}$ [a] in mbar	$\Delta p_{tt,41}$ [b] in mbar	$\Delta p_{tst,41}$ [b] in mbar	$\eta_{is,tt,81}$ [a] in %	$\eta_{is,tt,41}$ [b] in %	$\eta_{is,tst,41}$ [b] in %	P in W	ΔT_{tt} in K	Δs_{41} [b] in J kg^{-1} K^{-1}
Exp. [15]	0.14	1.96	64.5 ± 0.2	-	58.2 ± 3.1	47.8 ± 1.7	-	43.2 ± 1.5	16.8 ± 0.6	14.2 ± 0.5	-
FP	0.14	1.96	56.6	76.4	42.1	50.7	67.9	37.9	13.9	11.8	12.3
SP	0.14	1.96	**62.9**[c]	80.6	45.8	**54.8**[c]	69.7	40.2	14.3	12.1	11.9
SP	0.24	2.06	**30.0**[c]	40.0	19.0	**45.7**[c]	60.7	29.1	15.9	7.2	8.9
SP	0.14	1.96	**42.4**[c]	52.6	29.5	**58.1**[c]	71.8	40.6	17.6	7.9	7.0
SP	0.09	1.91	**51.8**[c]	64.0	39.5	**64.5**[c]	79.3	49.4	19.3	8.7	5.7
SP	0.04	1.86	**63.8**[c]	78.2	51.0	**73.0**[c]	88.9	58.6	20.9	9.4	3.3
SP	0	1.82	**69.7**[c]	85.0	58.2	**76.3**[c]	92.5	64.0	21.8	9.8	2.3

[a] Evaluated between the machine inlet (1) and machine outlet (8) [b] Evaluated between the machine inlet (1) and fan blade TE (4)
[c] Estimated with the volute pressure loss (4-8) according to eq. (8)

to the simulation of the hot air case. This leads to a rotational speed of 175.5 krpm and a mass flow rate of 4.71 kg h^{-1} which is slightly off-design. All other boundary conditions are similar (total inlet pressure of 0.96 bar and total inlet temperature of 200 °C). Equation (14) suggests that the total-to-total pressure rise is lower for the anode off-gas case.

The simulated total-to-total pressure rise is 63.8 mbar for the anode off-gas at the nominal tip clearance case (0.4 mm). It, therefore, is 5 mbar lower than the hot air SP simulation at the nominal clearance. As a result, the fan power is also lower (0.8 W). Additionally, the specific heat capacity of the anode off-gas (1.5 J kg^{-1} K^{-1}) is higher compared to the hot air (1.0 J kg^{-1} K^{-1}); hence, the temperature rise over the machine is lower and an experimental determination of the exact power and efficiency is more challenging, due to the measurement uncertainty and possible heat fluxes. In comparison to the hot air with the nominal tip clearance, the isentropic efficiency calculated with eq. (11) is increased by 13.7 % points, since the recirculation fan was designed for the operation with the anode off-gas. With respect to the initial blade tip clearance (0.14 mm), the pressure rise and efficiency are increased by 50 % and by 26 %, respectively, for the nominal tip clearance. For the theoretical case with a blade tip clearance of 0, the fan pressure rise and efficiency are 70 mbar and 76 %, respectively, highlighting therefore the high impact of the tip clearance on the fan performance.

Comparison of hot air and anode off-gas case: Figure 4 shows a comparison of the decrease of the total-to-total isentropic isentropic efficiency ($\eta_{is,tt,81}$) with respect to the relative blade tip clearance (S_4/H_4), using the 0.022 case as reference efficiency, i.e., 64 % and 73 % for the anode off-gas and the hot air case, respectively. For the 0.022 relative blade tip clearance, the decrease of efficiency for the anode off-gas and the hot air cases can be approximated with a gradient of -1.5 and -0.9, respectively. The experience coefficient (ζ) in eq. (1) is lower for the hot air case, indicating less sensitivity to an increased tip clearance. It is 2.1 ($1.5/0.73$) for the anode off-gas and 1.4 ($0.9/0.642$) for the hot air. The anode off-gas and hot air cases in Figure 4 can be approximated with a linear function of $y = -2.3x + 0.03$ and $y = -1.8x + 0.02$, respectively. Thus, the experience coefficient (ζ) in eq. (1) is 3.1 ($2.3/0.73$) and 2.8 ($1.8/0.64$), respectively. The experimental measurements for hot air (green lines) corroborate well with trend. As indicated by Brasz [16], the blade tip clearance loss becomes less significant for large tip clearances. Considering hot air, the slope in Figure 4 reduces from -2.63 (between 0.049 and the 0.077 relative blade tip clearance) to -1.67 (between 0.077 and 0.132). For the anode off-gas, this reduction is less significant (from -2.33 to -2.25, indicating a linear trend). The decrease in total-to-total isentropic

Copyright © 2020 by ASME

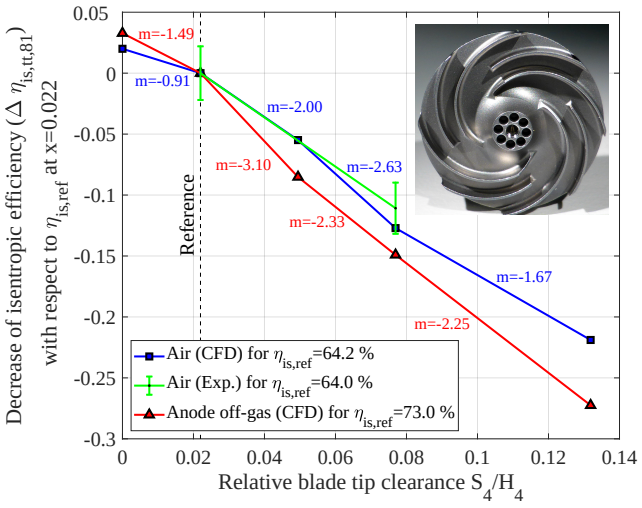

FIGURE 4: CHANGE OF THE FAN TOTAL-TO-TOTAL ISENTROPIC EFFICIENCY WITH RESPECT TO THE REFERENCE ISENTROPIC EFFICIENCY AT A RELATIVE BLADE TIP CLEARANCE OF 0.022 FOR THE SIMULATED ANODE OFF-GAS CASE (RED TRIANGLES) AND THE SIMULATED (BLUE SQUARES) AND MEASURED (GREEN ERRORBARS) AIR CASE. THE DIFFERENT SLOPES (M) ARE INDICATED AND RANGE BETWEEN 0.9 AND 3.1. THE FAN TE BLADE HEIGHT (H_4) IS 1.82 mm AND THE DIAMETER (d_4) IS 19.2 mm.

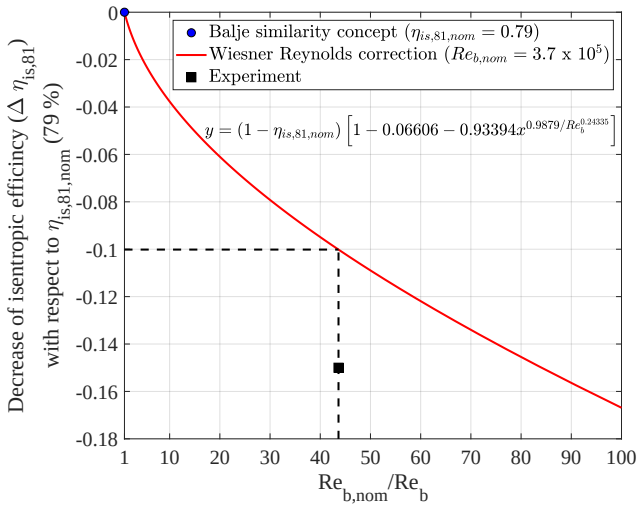

FIGURE 5: DECREASE OF THE TOTAL-TO-STATIC ISENTROPIC EFFICIENCY OF 79 % AT $n_s = 0.84$ AND $d_s = 4.15$ (FIGURE 3.7 IN BALJE [17]) WITH THE REYNOLDS LOSS CORRECTION ACCORDING TO THE EMPIRICAL EQUATION OF WIESNER [18] FOR A $Re_{b,nom} = 3.7 \times 10^5$. THE CORRECTED EFFICIENCY FOR THE PRESENTED FAN ($Re_b = 8.5 \times 10^3$) IS 69 %, AND THUS 5 % POINTS HIGHER THAN THE ACTUAL MEASURED VALUE (64 %).

efficiency over the whole machine for the hot air and anode off-gas at 200 °C (design case)

$$\Delta\eta_{is,tt,81} = -1.8\frac{S_4}{H_4} \qquad \text{Air} \qquad (15)$$

$$\Delta\eta_{is,tt,81} = -2.3\frac{S_4}{H_4} \qquad \text{Anode off-gas} \qquad (16)$$

can be approximated with a linear function that fits the numerical and experimental results within ±2 % points. The Reynolds number (Re_d) is 1.2×10^5 and 0.9×10^5 for anode off-gas and hot air, respectively.

COMPARISON OF THE EXPERIMENTAL RESULT TO SIMILARITY CONCEPTS BY BALJE AND REYNOLDS CORRECTION

Considering the hot air case with the nominal clearance of 0.04 mm at the experimental conditions ($p_{t,1} = 0.96$ bar, $T_{t,1} = 200$ °C, $\dot{m} = 5.3\,\mathrm{kg\,h^{-1}}$, and $n_{rot} = 168$ krpm), the specific speed and the specific diameter

$$n_s = \omega\frac{\sqrt{\dot{V}_1}}{\Delta h_{is,tst}^{0.75}} \qquad (17)$$

$$d_s = d_4\frac{\Delta h_{is,tst}^{0.25}}{\sqrt{\dot{V}_1}} \qquad (18)$$

correspond to 0.84 and 4.15, respectively, resulting in a to a total-to-static isentropic efficiency of 79 % according Balje [17] (figure 3.7). This is significantly higher than the measured value of 64 %. The tip clearance effect is negligible, since Balje assumes a value of 0.02 for the relative tip clearance (S_4/H_4), whereas the investigated fan has a value of 0.022. However, the Reynolds number based on the tip diameter (Re_d) is much lower: Balje's similarity concepts are based on a Reynolds number of 2×10^6, whereas the Reynolds number of the investigated fan is 0.088×10^6, and thus 23-times lower. Thus, the Reynolds effect is supposed to have a significant impact on the measured fan efficiency. Wagner et al. [19] suggested to correct the predicted efficiencies with the Wiesner correlation.

In 1979, Wiesner [18] reviewed several efficiency correction equation based on Reynolds losses, ranging from the year of

Copyright © 2020 by ASME

1925 until 1974. All of these correlations are based on the equation as follows

$$\frac{1-\eta_{is}}{1-\eta_{is,nom}} = \zeta_1 + (1-\zeta_1)\left(\frac{Re_{nom}}{Re}\right)^{\zeta_2} \tag{19}$$

with two empirical experience coefficients (ζ_1 and ζ_2). The coefficient ζ_1 ranges between 0 and 0.57 and ζ_2 between 0.1 and 0.5. Wiesner defined the parameter ζ_1 to 0.06606 and ζ_2 as a function of the Reynolds number ($0.9879/Re_b^{0.24335}$). He suggested to utilize the Reynolds number based on the TE channel width (Re_b) in accordance with the ASME PTC-10 performance test code, instead of the tip diameter (Re_d). The nominal Reynolds number in eq. (19) can be computed with the nominal TE channel width.

$$Re_{b,nom} = 1.595 \times 10^7 b_{4,nom} \tag{20}$$

Thus, in order to utilize Wiesner's efficiency correction, the channel width of the nominal geometry needs to be known.
For Balje's similarity concepts at $n_s = 0.84$ and $d_s = 4.15$, the channel width is estimated to be 23.3 mm, using the fan total-to-static enthalpy difference ($\Delta h_{is,tst}$), the Reynolds number based on the tip diameter ($Re_d = 2 \times 10^6$), the relative blade tip clearance ($S_4/H_4 = 0.02$), and the blade height to tip diameter ratio ($H_4/d_4 = 0.1$, figure 6.55). The nominal Reynolds number based on the TE channel width (Re_b), according to eq. (20), is thus 3.7×10^5. Since the value of Re_b is 8.5×10^3 for the tested fan, the $\frac{Re_{b,nom}}{Re_b}$ ratio is 43.5. This is equal to an efficiency correction of 10 % (Figure 5), which corresponds to an predicted total-to-static isentropic efficiency of 69 %. In contrast, the experimentally measured value is 5 % points lower (65 %). However, Balje assumes a three-dimensional impeller geometry with zero incidence, a mixed-flow impeller (88°), and a diffuser after the TE, whereas the presented fan has prismatic blades (Figure 4), is radial, and the flow exits directly into the volute, and thus leading to an increased pressure losses. The authors, therefore, conclude that the similarity concepts by Balje are valid for the preliminary design of such a micro fan, if the efficiency correction based on the Reynolds effect is taken into consideration. If the relative tip clearance is higher than 0.02, the tip clearance correction according to eq. (15) needs to be considered.

DESIGN GUIDELINES

Due to the manufacturing and assembling tolerances, the relative blade tip clearance is typically higher for small-scale turbomachines. Thus, the blade tip clearance leakage loss is more significant, also for fans with relatively low pressure rises. The authors suggest therefore the following measures to reduce this secondary loss:

- Accurate journal bearings to realize tight tip clearances (here: tip clearance of 0.05 mm, realized with dynamic gas film bearings, i.e., herringbone-grooved journal bearings, that have a bearing clearance of 0.01 mm).
- Thrust bearings with a low axial motion (here: single-sided spiral-grooved thrust bearing, with an estimated maximum motion of 0.01 mm).
- Mitigating the onset of the tip leakage vortex by unloading the blade front (here: zero-Euler-work blade design at the first 22 % of the meridional coordinate).
- Mid-loaded blade loading, as suggested by Diehl [11] for low-Reynolds number radial compressors.
- Carefully designed main and splitter blades to guide the tip leakage vortices along the blade suction side through the blade channel, as suggested by Diehl [11].

CONCLUSION

The blade tip clearance effect for a 19.2 mm radial fan was studied numerically and experimentally. With respect to the measurements (rotational speed of 168 krpm, air mass flow rate of 5.3 kg h^{-1}, and total inlet temperature of 200 °C), the total-to-total pressure rise could be increased by 20 mbar to 68 mbar, while the power increased from 19 W to 22 W, by reducing the clearance from 0.14 mm to 0.04 mm. Thus, the isentropic total-to-total efficiency increased from 53 % to 64 %. The fan impeller efficiency is estimated to be 79 %, which is high, considering the low Reynolds number based on the tip diameter (0.9×10^5), the low flow coefficient (0.035), and the simple two-dimensional blade design. Efficiencies towards 79 % could be achieved by adding a pinched diffuser. However, this would increase the system complexity and size.
A single passage CFD simulations correlates well to the experiments with a relative blade tip clearance (based on the blade height) of 0.022 and 0.077. Correlations from the literature were compared towards the numerical results, suggesting only accurate correlation with the model from Pfleiderer with an experience coefficient of 3.1 (anode off-gas) and 2.8 (hot air). Pfleiderer [5] reports, that for small blade tip clearances, the isentropic efficiency can increase with increasing blade tip clearance, before it starts to decrease. Schmidt-Theuner and Mattern [6] and Musgrave [7] suggest negligible impact of the relative blade tip clearance below values of 0.035 and 0.03, respectively. For the presented fan, a lower impact was observed for a relative blade tip clearance of 0.022. Here, an experience coefficient of 2.1 (anode off-gas) and 1.4 (hot air) fit the numerical results.
Similarity concepts by Balje are suggested to be valid for the pre-design of such a micro fan. However, the designer needs to carefully evaluate the significant effects of a possibly increased relative blade tip clearance and/or the increased profile losses, due to a decreased Reynolds number. The efficiency correction equation by Wiesner [18] is suggested to be appropriate for this

Copyright © 2020 by ASME

case.
The authors proposed general guidelines for the design of a small-scale fan. These guidelines allow to design an efficient baseline fan. However, parameters, such as the exact positioning of the splitter blade leading edge or the exact loading distribution need to be further refined during the design process, e.g., with an single passage computational fluid dynamic simulation. No exact values can be stated; this would need a more thorough analysis with different fan geometries.

ACKNOWLEDGMENT

The authors acknowledge the investigation by Conti Romain and Luca Massera in the frame of two semester projects, as well as the discussions and suggestions by Adeel Javed and Markus Diehl. This work is supported by the research grant from the Canton de Vaud under the "100 million de francs pour les energies renouvelables et l'efficacite energetique" and the Horizon 2020 Research and Innovation Programme under Grant Agreement No. 815284.

REFERENCES

[1] Schiffmann, J., and Favrat, D., 2010. "Design, experimental investigation and multi-objective optimization of a small-scale radial compressor for heat pump applications". *Energy,* ***35***(1), Jan., pp. 436–450.

[2] Sato, S., Jovanovic, S., Lang, J., and Spakovszky, Z., 2011. "Demonstration of a Palm-Sized 30 W Air-to-Power Turbine Generator". *Journal of Engineering for Gas Turbines and Power,* ***133***(10), May, pp. 102301–102311.

[3] Diehl, M., Schreiber, C., and Schiffmann, J., 2019. "The role of Reynolds number effect and tip leakage in compressor geometry scaling at low turbulent Reynolds numbers". *Journal of Turbomachinery*, Nov., pp. 1–14.

[4] Eckert, B., and Schnell, E., 1953. *Axial- und Radialkompressoren*. Springer, Berlin.

[5] Pfleiderer, C., 1955. *Die Kreiselpumpen für Flüssigkeiten und Gase: Wasserpumpen, Ventilatoren, Turbogebläse, Turbokompressoren*. Springer, Berlin.

[6] Schmidt-Theuner, P., and Mattern, J., 1968. "The effect of Reynolds number and Clearance in the centrifugal compressor of a turbocharger". *The Brown Boveri Review,* ***55***(8), pp. 453–456.

[7] Musgrave, D. S., 1980. "The prediction of design and off-design efficiency for centrifugal compressor impellers". In Performance Prediction of Centrifugal Pumps and Compressors, pp. 185–189.

[8] Pampreen, R. C., 1973. "Small Turbomachinery Compressor and Fan Aerodynamics". *Journal of Engineering for Power,* ***95***(3), July, pp. 251–256.

[9] Ganter, M., 1985. "Experimentelle Untersuchungen des Spaltverlustes radialer Kreiselpumpen mit offenem Laufrad". Phd thesis, TU Braunschweig.

[10] Diehl, M., and Schiffmann, J., 2019. "Impact of large tip clearance ratios on the performance of a centrifugal compressor". In Proceedings of 13th European Conference on Turbomachinery Fluid dynamics & Thermodynamics.

[11] Diehl, M., 2019. "Mitigation of tip leakage induced phenomena in a low Reynolds number centrifugal compressor via blade loading distribution". PhD thesis. https://infoscience.epfl.ch/record/269163. Accessed: 2019-11-19.

[12] Javed, A., Arpagaus, C., Bertsch, S., and Schiffmann, J., 2016. "Small-scale turbocompressors for wide-range operation with large tip-clearances for a two-stage heat pump concept". *International Journal of Refrigeration,* ***69***, Sept., pp. 285–302.

[13] Wagner, P. H., Van herle, J., and Schiffmann, J., 2019. "Theoretical and Experimental Investigation of a Small-scale, High-speed, and Oil-free Radial Anode Off-gas Recirculation Fan For Solid Oxide Fuel Cell Systems". *Journal of Engineering for Gas Turbines and Power*.

[14] Bruno Eck, 2003. *Ventilatoren : Entwurf und Betrieb der Radial-, Axial- und Querstromventilatoren*, 6. aufl. ed. Springer, Berlin etc.

[15] Wagner, P. H., Wuillemin, Z., Constantin, D., Diethelm, S., Van herle, J., and Schiffmann, J., 2020. "Experimental Characterization of a Solid Oxide Fuel Cell Coupled to a Steam-Driven Micro Anode Off-Gas Recirculation Fan". *Journal of Applied Energy (accepted for publication)*.

[16] Brasz, J. J., 1988. "Investigation into the Effect of Tip Clearance on Centrifugal Compressor Performance". In Proceedings of the the Gas Turbine and Aeroengine Congress, Amsterdam, Netherlands - June 6-9, 1988.

[17] Balje, O. E., 1981. *Turbomachines : a guide to design, selection and theory*. Wiley, New York etc.

[18] Wiesner, F. J., 1979. "A new appraisal of Reynolds number effects on centrifugal compressor performance". *ASME Transactions Journal of Engineering Power,* ***101***, pp. 384–392.

[19] Wagner, P. H., Wuillemin, Z., Diethelm, S., Van herle, J., and Schiffmann, J., 2017. "Modeling and Designing of a Radial Anode Off-Gas Recirculation Fan for Solid Oxide Fuel Cell Systems". *Journal of Electrochemical Energy Conversion and Storage,* ***14***(1), May.

Copyright © 2020 by ASME